An experimental revisit of plasma phenomena on Helicon Plasma Thrusters

IEPC-2019-903

Presented at the 36th International Electric Propulsion Conference
University of Vienna, Austria
September 15-20, 2019

J. Navarro-Cavallé,[*] M. Wijnen,[†] P. Fajardo[‡] and E. Ahedo[§]
Equipo de plasmas y propulsión eléctrica (EP2), Universidad Carlos III de Madrid, Leganés, 28911, Spain

This work aims to describe the observed structures of the plasma beam exhausted by an Helicon Plasma Thruster. Experimental data has been acquired through an intense experimental campaign on the HPT05M prototype, which has been operated nominally at 20 sccm of Argon, 450 W of RF power, and magnetic field strengths about 1000 G. This work explores the impact of these operating parameters on the plasma plume structure. Among these structures, special attention is invested on the analysis of the ion energy distribution function. The second part is devoted to explore the radial or azimuthal profiles for other plasma properties, such as the density, the electron temperature, and the plasma potential.

I. Introduction

The Helicon Plasma Thruster (HPT) has been presented as a disruptive electric thruster for in-space propulsion from beginnings of 2000 [1–3]. Almost two decades later, some institutions start to show HPT prototypes at relative high TRL [4,5], although their performances are far from other mature technologies at the same power levels. The bibliography on HPT has become large too, including from theory to ready-to-fly prototypes datasheets, passing through experimental and numerical intense research. However, the disparity on the performances of the different prototypes tested up to date point out the lack of physical understanding on the main processes. On the other hand, there are not yet numerical tools able to perform a simulation of the whole phenomena taking place within a HPT: neutral gas ionization, magnetic confinement, rf-plasma coupling, plasma acceleration, etc., even for some processes, the description of each one isolated from others is still not reliable. Due to these existing uncertainties the design process of an optimized prototype is unclear. In this work, some important aspects on helicon plasma discharges are revisited from an experimental point of view. In Section II the experimental setup is described, mainly detailing the particularities of the HPT05M prototype and the set of diagnostics that have been used to acquire all the experimental data. Section III analyses the impact of the HPT operating parameters on the Ion Energy Distribution Function (IEDF). Section IV presents and discuss the on-axis, off-axis and azimuthal structures of the main plasma properties at the HPT05 plasma plume, including density, electron temperature, and plasma potential profiles. The last section summarizes and concludes on the main results of this work.

II. HPT experimental setup

The HPT device that has been explored in this research is the HPT05M prototype, Figure 1. This has been designed to operate at a nominal power of 450 W (@13.56 MHz). This is derived from a former

[*]Assistant Professor, Aerospace Engineering Department, jaume.navarro@uc3m.es
[†]PhD Student, Aerospace Engineering Department, mwijnen@pa.uc3m.es.
[‡]Associate Professor, Aerospace Engineering Department, pablo.fajardo@uc3m.es.
[§]Professor, Aerospace Engineering Department, eduardo.ahedo@uc3m.es.

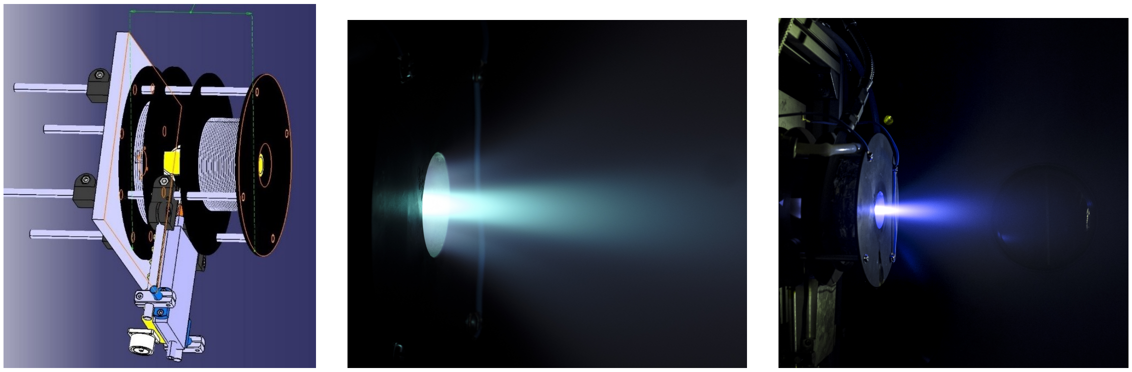

Figure 1. HPT5M prototype CAD draw (left) firing at 10 sccm of Xenon (centre) and 20 sccm of Argon (right), at 1500 G, and 450 W. The plasma beam is extremely well collimated.

prototype developed by UC3M and SENER Aeroespacial.[6,7] It has been operated with both Xenon and Argon as propellants, with a nominal mass flow rate of 10 and 20 sccm respectively for each gas. However, for the sake of shortness, results will be presented only for Argon. It has been checked that the qualitatively response of the HPT05M due to the modification of operating parameters is the same for either Xenon or Argon. The magnetic generator has been simplified in this work to the use of a single solenoid, which produces a magnetic topology in the shape of a convergent-divergent magnetic nozzle. The magnetic field strength goes from 0 to 1500 G approximately. The plasma discharge chamber consists of a quartz tube of about 150 mm length or less, depending on the position of the different Macor injectors that have been tested. The nominal diameter of the quartz tube is 25 mm inner diameter. The RF half-turn helical antenna, 75 mm length, has been placed just behind the solenoid, between it and the injector section. The antenna is fed by an unbalanced feeder. At the other side of the feeder, a $\pi-$type matching network was in charge of matching the antenna-plasma impedance to the 50 Ohm characteristic impedance of the power amplifier. A customized off the shelf (SEREN) power amplifier, 2 kW class, is used to generate the RF power.

In order to measure the plasma properties, a Retarded Potential Analyzer (RPA) has been used to acquire the ion energy distribution function (IEDF). Plasma density n, plasma potential ϕ and electron temperature T_e have been measured by means of a RF compensated Langmuir Probe (RFCLP), after postprocessing accurately the acquired characteristic $I-V$ curves.

All the mentioned intrusive plasma diagnostics have been mounted on a rotary arm system, that allows to scan the plasma properties in a 2D horizontal plane that contains the thruster axis. The arm centre of rotation is aligned with the centre of the thruster outlet section. r is the distance between this centre and the probe collecting surface. Probes can be moved along this r distance from 0 to 450 mm. Azimuthally, probes can be moved from $\alpha=-90,+90$, being α the angle between the thruster axis and the rotary arm.

III. Analysis of the Ion Energy distribution function

The IEDF has been acquired for different operating sets. Results for Argon are provided regarding the ion averaged energy and ion energy dispersion, as it can been seen in Figure 2. For the sake of completeness, smoothed IEDF curves, from which the results have been obtained, are also included in this document in Figure 3. These curves also allow identifying the ion energy of maximum probability. From these results, it is possible to assess the impact of (1) Argon mass flow rate, (2) magnetic field strength, and (3) magnetic field polarity, on the ion energy.

First, as the mass flow rate decreases down to 10 sccm (at constant power, 450 W, and magnetic field, 1500 G, red points in Figure 2 and bottom left plot in Figure 3), the ion energy of maximum probability as well as the ion averaged energy increase. This behavior agrees the recurrent thesis that at lower mass flow rates, ion energy increases due to reaching a higher electron temperature. This seems to be motivated by the higher propellant utilization and the lower collisions at low mass flow rates. However, the ion energy dispersion also increases at lower mass flow rates, and this could impact negatively on the overall thrust efficiency. The corresponding IEDF curves in Figure 3 show a very noisy behavior due to the lower ion current density. However, it is difficult to identify whether this ion energy dispersion arises from the existence of

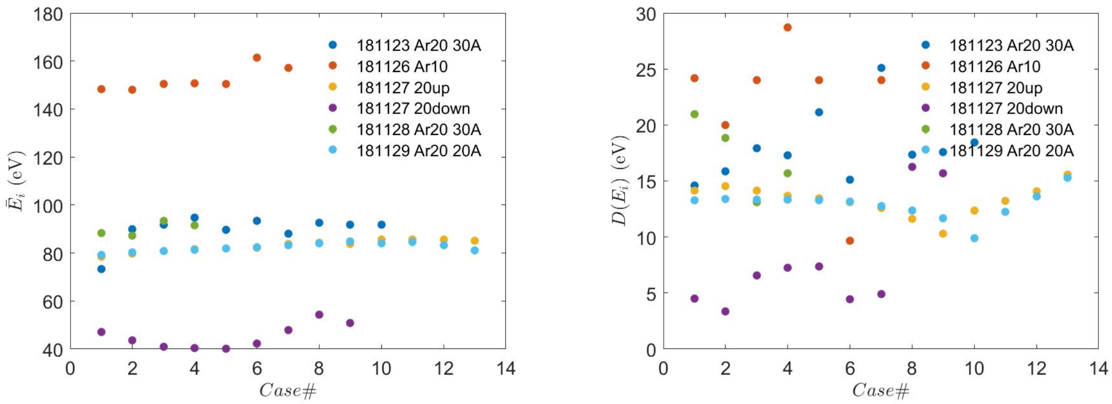

Figure 2. Ion averaged energy and ion energy dispersion, for the HPT05M prototype operated with Argon. Power is kept constant at 450 W, while mass flow rate and magnetic field are modified to analyze their impact. Case # refers to a different point of RPA acquisition (r radial position and and α the azimuthal position). Dark blue and green are for $B = 1500$ G and 20 sccm (# case 1 of blue line is for 1000 G). Light blue and yellow are for 20 sccm and 1000 G. Red dots are for 10 sccm and 1500 G. Violet dots are for 20 sccm and 1000 G, but inverted polarity.

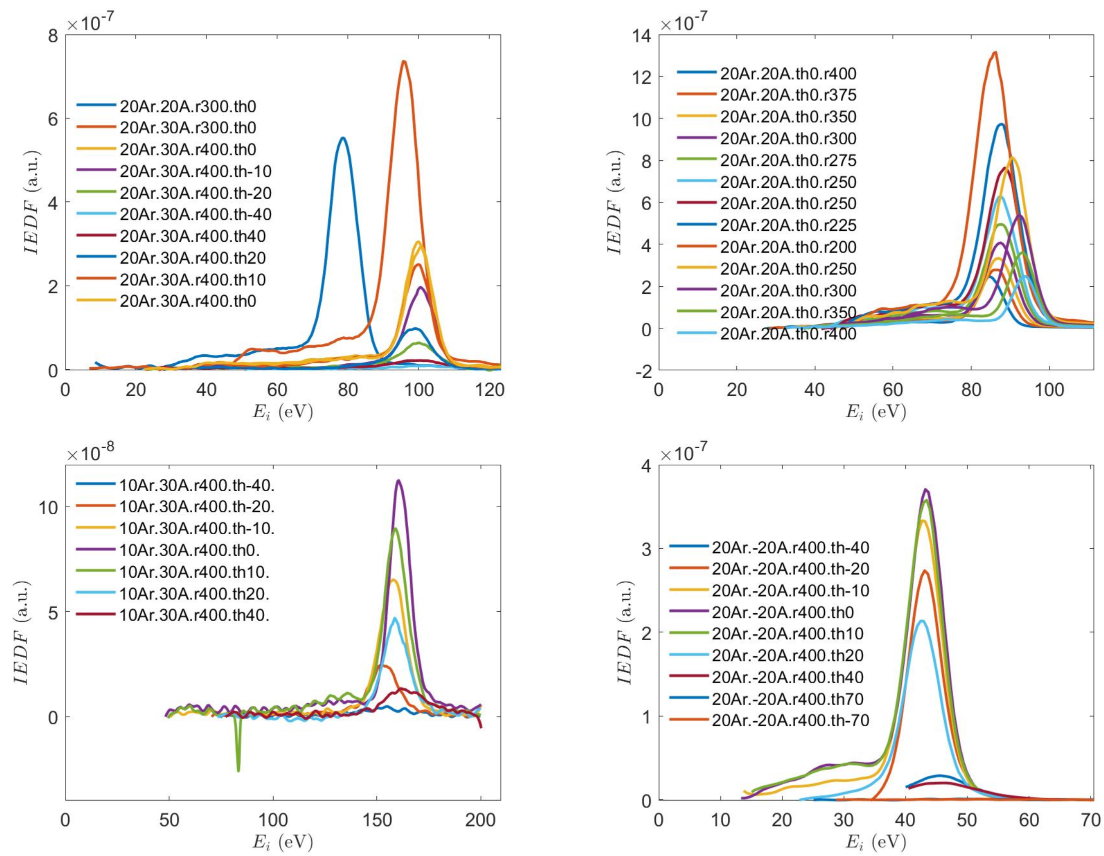

Figure 3. IEDF for some of the operating cases depicted in Figure 2. All operated with Argon at 450 W. Top left: 1500 G and 20 sccm (except the lower energy, blue line, in which $B = 1000$ G); top right: 1000 G and 20 sccm; bottom left: 1500 G and 10 sccm; and bottom right: 20 sccm and 1000 G with inverted polarity.

a two different populations (or non-negligible lower ion energy population, as observed for other HPT05M settings). A small asymmetry on the IEDF is also noticed along the angular direction, being the beam deviated (in terms of higher current) to positive angles, which is chosen to the left side of the plasma plume seen from the thruster exit.

Second, concerning the effect of rising up the magnetic field strength on the IEDF, there is an increase about 10-20 eV on the ion energy of max probability and the ion mean energy, when the magnetic field is increased from 1000 to 1500 G. This can be checked in Figure 2, dark and light blue, green and yellow markers. In terms of ion dispersion, it seems to rise up at the higher magnetic field. For the dark blue dots in Figure 2, the first case corresponds to a single measurement took at 1000 G, while the rest of the set was taken at 1500 G. This shows a clear example of the slight increase of ion energy with magnetic field strength. IEDF curves are presented in the top plots of Figure 3.

Third and last, the effect of the magnetic field polarity plays an important role on the achievement of a high energy ion beam. The ion energy drops dramatically when the magnetic field is reversed (inverted polarity but keeping constant the magnetic strength at 1000 G), from 80-90 eV down to 40-50 eV range. This result allows understanding the importance of both, magnetic field strength and field direction, on the efficiency of RF-power plasma coupling mechanisms. The ion flux is reduced as well, and RPA data becomes too noisy to be properly postprocessed at large azimuthal angles. The results for the inverted polarity can be seen in Figure 2, purple line, and Figure 3, bottom right plot.

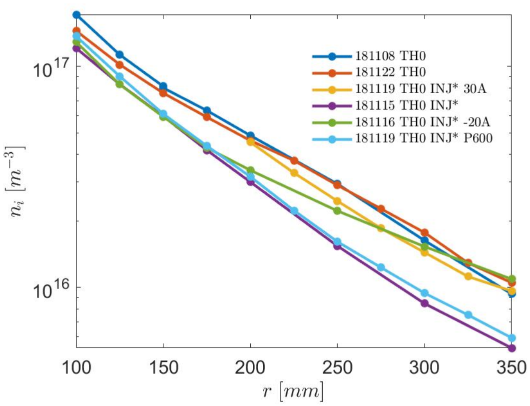

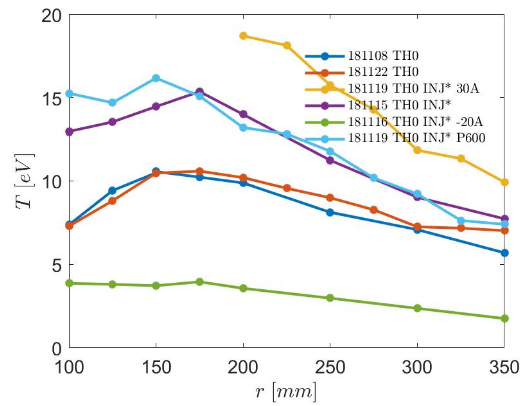

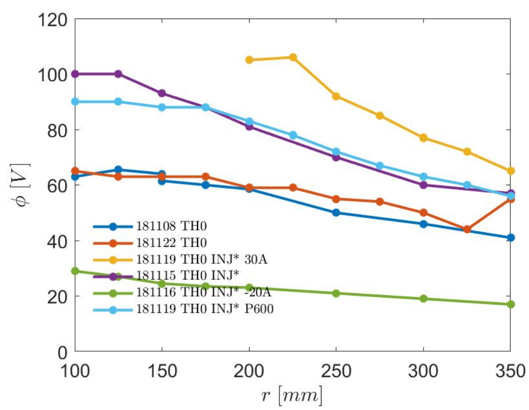

- 20181108 & 20181122 (nominal operating sets).
- 20181119 (INJ*, 1500 G).
- 20181119 (INJ*, S2=30 Amp) 20181115 (INJ* and nominal).
- 20181116 (INJ*, 1000 G and inverted polarity).
- 20181119 (INJ*, $P_{RF} = 600$ W).

Figure 4. HPT05M plasma beam structure, on-axis measurements of plasma density (top left), electron temperature (top right) and plasma potential (bottom left). Legend description for each case is on the list at the bottom right corner.

IV. Analysis of the plasma beam structure

Plasma density, electron temperature and plasma potential profiles have been explored for thruster different operating parameters. Most of the results concerning the mentioned plasma properties were taken at

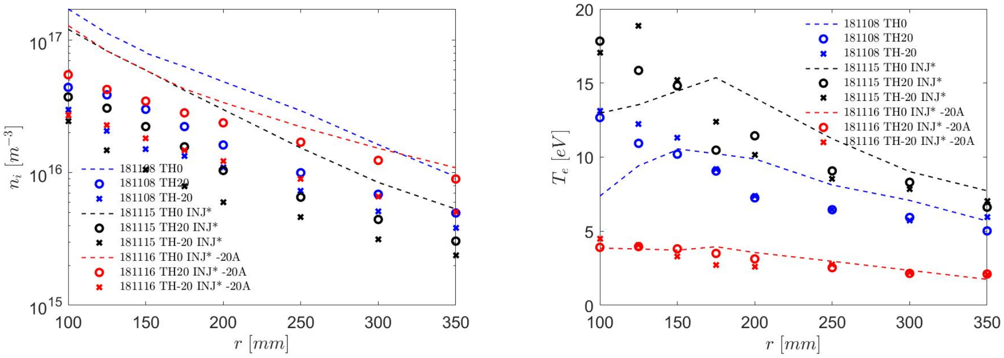

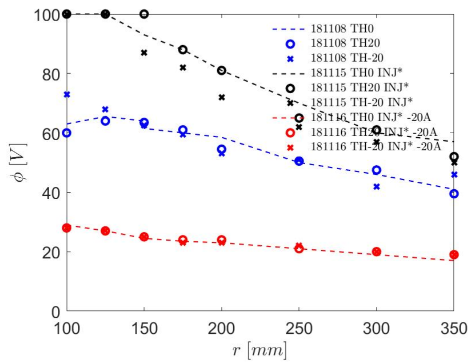

- 20181108 (nominal operating sets).
- 20181115 (INJ*).
- 20181116 (INJ*, 1000 G with inverted polarity).

Figure 5. HPT05M plasma beam structure, off-axis measurements (±20) of plasma density (top left), electron temperature (top right) and plasma potential (bottom left). Legend description for each case is on the list at the bottom right corner.

the HPT05 axis line ($\alpha = 0$). Later, results will be presented for scans taken at $\alpha = \pm 20$ deg and $\alpha = \pm 40$ deg. The nominal scenario is for 450 W, 20 sccm of Argon and 1000 G, otherwise, modifications on the configuration/operating sets will be announced in the legend of each plot. The nominal injector measures 25 mm in diameter with a central hole for gas injection of about 1.5 mm in diameter. This injector fits perfectly with the quart tube. However in some tests an injector of 20 mm in diameter has been implemented and used. This allows loosing neutral gas and plasma from the region of discharge to the back, as a 30 % of the back face is uncovered by the Macor injector. Hereafter, in the corresponding plots and in the main text, the label INJ* will be used to refer to this second injector.

Concerning the on-axis plasma density profile, there are some interesting results that deserve to be further explained. First, the consistency on the measurements repeatability for the 181108-181122 data sets, Figure 4. These two sets present the highest density close to the HPT05 exit (i.e. 100 mm from the front face of the solenoid). For the 181119 data set (yellow line), which corresponds to tests performed at 1500 G, I-V raw data cannot be postprocessed successfully at distances shorter than 200 mm. The problem appears because the current drive into the RFCLP exceed the current that the DAQ (current meter) can manage before reaching the plasma potential voltage. Consequently, it could be stated that for this high magnetic field scenario, the density could be even larger. Note that the last mentioned case belongs to the subgroup of tests carried out with the modified injector, INJ*, so even the losses of plasma/neutral gas at the back part of the tube, the density level is in the same order than in the 181108 tests (with the nominal injector). Besides, the couple of tests 181115 (purple) and 181119 (light blue), performed at 1000 G, show a very similar response for all plasma properties, although 181119 was performed at a larger RF power, 600 W. This result is really interesting, for the high power case, the excess of power is not converted into neither higher plasma density, nor higher electron temperature, nor higher plasma potential. This means that the HPT05M configuration (at least working with Argon) is sized/optimized properly in terms of power (nominal at 450 W) at the nominal mass flow rate (20 sccm), and consequently the increase of power does not impact strongly on the HPT05M performances. Interestingly, these two last cases (1000 G, INJ*) together with 181119 (1500 G, INJ*), which has gas losses at the back part, present a higher temperature (and also potential) in comparison to the nominal case (closed tube at its back). This adds a new ingredient on the comprehension of what makes, or in other words, which design allows reaching a higher electron temperature. Previously to these results, the fact of reaching a higher temperature was linked to the proved fact of reaching a larger propellant utilization efficiency. However, this is not the case now. A reasonable explanation for the present behavior is that the partially-open tube at its back part, allows reducing somehow the electron collisionality due to the loss of propellant (flowing backward). This could have two implications, first to decrease the transport of plasma across the magnetic field, thus reducing energy losses, and keeping a higher temperature. Second, a reduction of the *inelastic* electron collisions imply that more energy is available for heating up the electrons. In any case, this requires a further analysis. The last case, 181116, was performed with an inversed field polarity, keeping the same strength, 1000 G. Density levels close to the thruster are similar to those measured for other INJ* configuration, but the curve deviates beyond 200 mm, showing a lower density decay. In fact, in the far field, density reaches the same values of denser cases (181108 and 181122). However, the measured temperature and plasma potential drops dramatically. These data together with that reported in Figures 2-3, concerning the IEDF, allows to ensure that in this configuration the ion beam formation/acceleration becomes poor. Indeed, the polarity of the field in this setup configuration is a key element on the plasma-wave coupling mechanism.

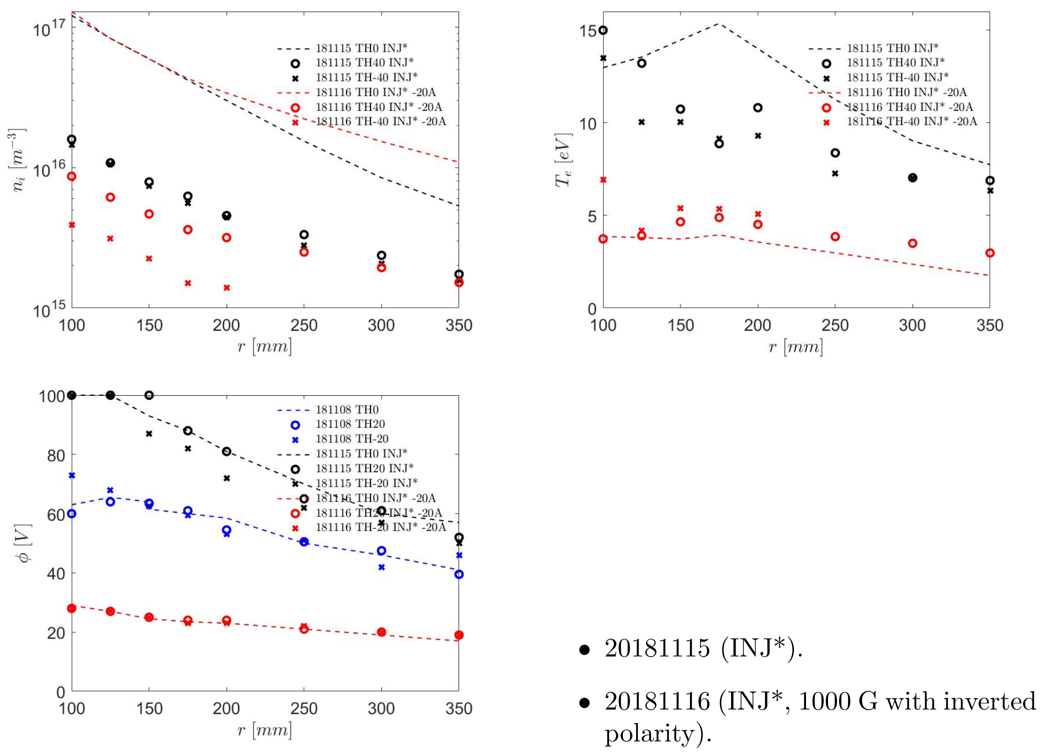

Figure 6. HPT05M plasma beam structure, off-axis measurements (±20) of plasma density (top left), electron temperature (top right) and plasma potential (bottom left). Legend description for each case is on the list at the bottom right corner.

Similar figures are presented for off-axis scans, at $\alpha = \pm 20$ deg in Figure 5 and $\alpha = \pm 40$ deg in Figure 6. Results are only presented for three cases: the nominal one (181108, as before), the nominal configuration using the injector INJ* (181115) and the one with inverted polarity (181116). Off-axis density profiles show a lower density than that measured on-axis (dashed lines). They also show an important asymmetry, higher densities are measured at +20 deg (open circles) in comparison to that at -20 deg (crosses). A possible misalignment of the probe/thruster setup could be considered a responsible for this differences. However, the density difference is in some cases too large to attribute this response just to setup misalignments. So, this could arise due to asymmetries on the plasma itself. Another remark appears on the off-axis electron temperature profile. Unlike in the on-axis measurements, at ±20 deg, the electron temperature does not present any peak, and this decreases monotonically in the downstream direction. In comparison to the density, both electron temperature and plasma potential do not show any important asymmetry, in fact, at some distances from the thruster they show a good agreement.

At ±40 deg off-axis, asymmetries on the plasma density appear again, but only for the case in which the magnetic field polarity is inverted. For this same case, a light peak on the electron temperature appears again. For the same case (20181116 INJ*), measurements at -40 deg and beyond 250 mm downstream of the HPT, have not been considered in the analysis since they cannot be postprocessed according any known LP theory due to the bad quality of the acquired raw data.

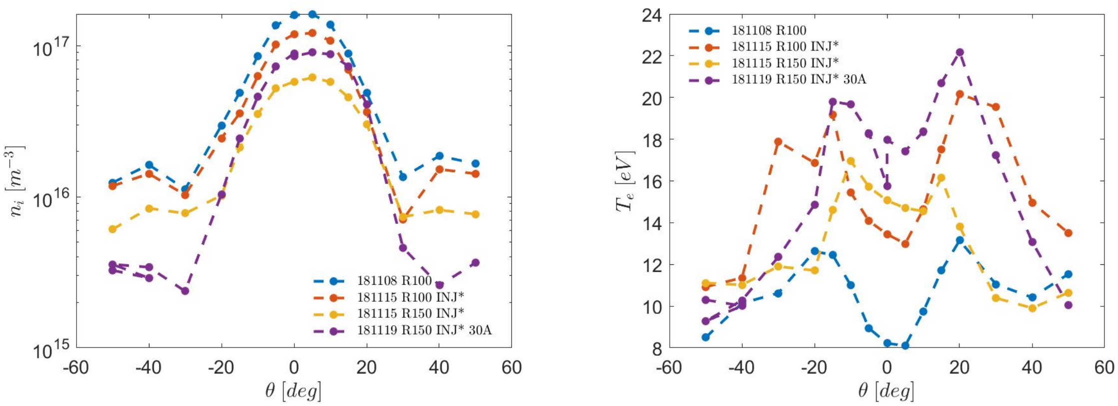

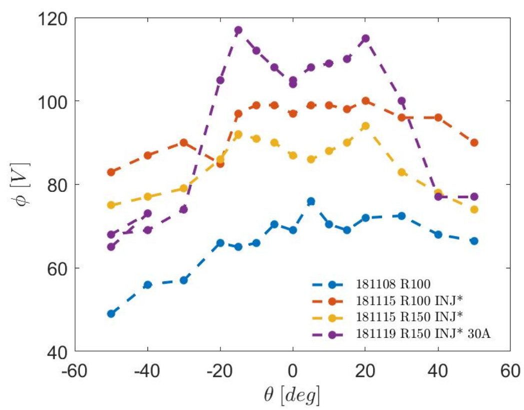

- 20181108, at $r = 100$ mm
- 20181115 (INJ*), at $r = 100 - 150$ mm.
- 20181116 (INJ*, 1500 G), at $r = 150$ mm.

Figure 7. HPT05M plasma beam structure, azimuthal measurements (at constant r) of plasma density (top left), electron temperature (top right) and plasma potential (bottom left). Legend description for each case is on the list at the bottom right corner.

Finally, Figure 7 summarizes the plasma properties measured at different azimuthal positions, ±50 deg, and constant radius ($r = 100 - 150$ mm depending on each case). Concerning the density profiles, most of the plotted curves show a similar behavior, a single peak, with a "symmetric" decay of at least one order of magnitude at an angle about ±30 deg. At larger angles the trend of the profile shows a slight increase of the measured plasma density. The modified setup implementing the injector INJ*, 181115 datasets (yellow and red dashed lines in the mentioned figure), shows similar density profiles, in comparison to the nominal case, 181108. This means that the loss of mass at the back does not impact to much on the density measured downstream of the thruster. This is somehow a controversial result that would require further analysis. The role of the magnetic field on the plasma density depletion at the beam wings is evident, just compare the case 181119 (1500 G, INJ*) against the 181115 case (1000 G, INJ*). It is noted that in the high magnetic field scenario, plasma density almost drops two orders of magnitude at the beam wings. Regarding temperature profiles, the authors point out that the uncertainty on the electron temperature measurements is large, in the order of ±2 eV. This problem arises because the aforementioned problem on the DAQ system, it saturates in current before reaching the plasma potential (i.e. inflection point of the I-V characteristic Langmuir probe). Indeed, it is a cumbersome task to postprocess all this data, and in some cases it is necessary to postprocess each individual case, at each probe position, separately, and the automatic algorithm has to be reviewed for this anomalous I-V data. The trend of the temperature profile is similar in all the analyzed cases. At the center of the plasma beam there is a depression in the electron temperature. The temperature rises at intermediates angles, reaching a peak at ±15 to ±25 deg, and then decreases again at larger angles. This result is again very interesting. Let us to assume that density profiles and temperatures are linked through the magnetic lines with the inner plasma source, or in other words, the plasma properties measured downstream keep some history from the region where the plasma has been produced and heated up. If this is true, it means that higher density regions are decoupled from higher temperature regions, and consequently the regions of higher plasma production (higher ionization - higher plasma density) could be decoupled from the region of stronger plasma-wave coupling (higher temperature). Known models on HPT theory are far away of facing this kind of complex problems.

Plasma potential profiles have a resemblance with the electron temperature profiles for cases 181115 (at $r = 150$ mm) and 181119. For cases at $r = 100$ mm, the profile does not show any double peak, and it looks asymmetric, lower potential at negative azimuthal angles. This asymmetry is also present in the global trend of the temperature profile for these cases measured at 100 mm.

V. Conclusions

This work has explored the IEDF and plasma structure at the plume of the HPT05M prototype. The impact of the operating parameters, mass flow rate, and magnetic field, on the IEDF has been explored pointing out the high increase of the ion energy when the mass flow rate is decreased. The increase of the the magnetic field strength in the 1000-1500 G range seems to play a minor role on the IEDF. On the other hand, a good choice of the magnetic polarity is the key point to couple RF power effectively to the generated plasma. On-axis and off-axis results concerning plasma density, electron temperature and plasma temperature have been analyzed. Finally, the azimuthal structure of the plasma beam has been investigated. A different trend between the density and temperature profiles has been identified, concluding that regions of higher ionization, i.e. higher plasma density, are decoupled from the region of higher electron temperature. The role of the magnetic field on the formation of secondary plasma structures at the beam periphery has been described. This work presents an interesting snapshot of the plasma plume structure at the MN of an HPT, the HPT05M prototype. These results are very valuable for modelling verification since the presented plots show part of the plasma phenomena realm, pointing out the complexity of the different plasma structures.

Acknowledgments

This work has been partially supported by Project ESP2016-75887 (Spain's National Research and Development Plan - MINECO/FEDER). The authors acknowledge the support of SENER Aeroespacial on the development of the HPT05M breadboard.

References

[1]West, M., Charles, C., and Boswell, R., "Testing a helicon double layer thruster immersed in a space-simulation chamber," *Journal of Propulsion and Power*, Vol. 24, No. 1, 2008, pp. 134–141.

[2]Batishchev, O., "Minihelicon Plasma Thruster," *IEEE Transaction on Plasma Science*, Vol. 37, 2009, pp. 1563–1571.

[3]Pavarin, D., Ferri, F., Manente, M., Curreli, D., Guclu, Y., Melazzi, D., Rondini, D., Suman, S., Carlsson, J., Bramanti, C., Ahedo, E., Lancellotti, V., Katsonis, K., and Markelov, G., "Design of 50W Helicon Plasma Thruster," *31th International Electric Propulsion Conference, Ann Arbor, Michigan, USA*, edited by F. Electric Rocket Propulsion Society, IEPC 2009-205, 2009.

[4]Siddiqui, M. U., Cretel, C., Synowiec, J., Hsu, A. G., Young, J. A., and Spektor, R., "First performance measurements of the phase four RF thruster," *International Electric Propulsion Conference*, 2017.

[5]Trezzolani, F., Manente, M., Toson, E., Selmo, A., Magarotto, M., Moretto, D., Bos, F., De Carlo, P., Melazzi, D., and Pavarin, D., "Development and testing of a miniature helicon plasma thruster," *35th international electric propulsion conference, Atlanta, Georgia, USA. IEPC-2017-519*, 2017.

[6]Navarro-Cavallé, J., Wijnen, M., Fajardo, P., and Ahedo, E., "Experimental characterization of a 1 kW helicon plasma thruster," *Vacuum*, Vol. 149, 2018, pp. 69–73.

[7]Navarro-Cavallé, J., Wijnen, M., Fajardo, P., Merino, M., Ahedo, E., Ruiz, M., and Gómez, V., "Experimental performances of a 1 kW HPT by means of plasma diagnostics," *35th International Electric Propulsion Conference, IEPC-2017-447 (Electric Rocket Propulsion Society, Fairview Park, OH, 2017)*, 2017.